Regional and seasonal variations of the Twomey indirect effect as observed by the ATSR-2 satellite instrument

Claire E. Bulgin,[1] Paul I. Palmer,[1] Gareth E. Thomas,[2] Christopher P. G. Arnold,[2] Elies Campmany,[2] Elisa Carboni,[2] Roy G. Grainger,[2] Caroline Poulsen,[3] Richard Siddans,[3] and Bryan N. Lawrence[3]

Received 1 August 2007; revised 26 October 2007; accepted 6 December 2007; published 26 January 2008.

[1] We use satellite observations of aerosol optical depth τ_a and cloud effective radius r_e from the ATSR-2 instrument in 1997 to investigate the Twomey indirect effect (IE, $-\partial \ln r_e/\partial \ln \tau_a$) in regions of continental outflow. We generally find a negative correlation between τ_a and r_e, with the strongest inverse relationships downwind of Africa. North American and eastern Asian continental outflow exhibits a strong seasonal dependence, as expected. Global values for IE range from 0.10 to 0.16, consistent with theoretical predictions. Downwind of Africa, we find that the IE is unphysically high but robust ($r = -0.85$) during JJA associated with high aerosol loading, and attribute this tentatively to the Twomey hypothesis accounting only for a limited number of physical properties of aerosols.
Citation: Bulgin, C. E., P. I. Palmer, G. E. Thomas, C. P. G. Arnold, E. Campmany, E. Carboni, R. G. Grainger, C. Poulsen, R. Siddans, and B. N. Lawrence (2008), Regional and seasonal variations of the Twomey indirect effect as observed by the ATSR-2 satellite instrument, *Geophys. Res. Lett.*, *35*, L02811, doi:10.1029/2007GL031394.

1. Introduction

[2] Atmospheric aerosols represent one of the largest uncertainties in current understanding of Earth's climate [*Intergovernmental Panel on Climate Change* (*IPCC*), 2007]. Aerosols affect the atmospheric radiation balance by absorbing and scattering solar radiation (direct effect), the magnitude of such effects depends on a number of factors including chemical composition, size distribution, and mixing state. Aerosols also affect cloud radiative properties by acting as cloud condensation nuclei, CCN (indirect effects, IE), depending on size and chemical composition. Assuming constant liquid water content (LWC), elevated concentrations of aerosols increase the cloud droplet number and subsequently reduce the mean cloud droplet size, leading to an increase in cloud albedo [*Twomey*, 1974]. Reduced cloud droplet size suppresses precipitation and increases cloud lifetime [*Albrecht*, 1989]. Accurate modelling of these indirect effects involves detailed aerosol microphysics, and is therefore difficult to use in large-scale chemistry-climate models [*IPCC*, 2007].

[3] There are a number of anthropogenic and natural sources of aerosols [*Seinfeld and Pandis*, 1998]. The main sinks of aerosols are gravitational settling and wet deposition, the relative importance of these depends on the aerosol physical and chemical properties, leading to lifetimes of typically a few days. Such short lifetimes lead to rapid spatial and temporal variations in loading and chemical composition that are not well suited for study by sparse ground-based measurement networks. Satellite observations offer a global perspective but currently they only measure a small number of aerosol and cloud optical properties, e.g. optical depth and single scattering albedo [*IPCC*, 2007]. A number of previous studies using data from satellite sensors show an inverse correlation between aerosol optical depths (used as a proxy for aerosol number) and cloud droplet properties in continental outflow e.g., *Avey et al.* [2007] or globally [e.g., *Breon et al.*, 2002].

[4] Here, we use satellite observations of aerosol and cloud optical properties from the Global Retrieval of ATSR Cloud Parameter and Evaluation (GRAPE) dataset [*Watts et al.*, 2000; *Marsh et al.*, 2004], to quantify the Twomey IE, as discussed below. In this analysis we use cloud droplet effective radius, r_e, the area weighted mean radius of cloud droplets, and aerosol optical depth, τ_a, a measure of total column light extinction due to scattering and absorption of aerosol particles.

2. Data

[5] The second Along-Track Scanning Radiometer (ATSR-2), aboard the ERS-2 satellite, observes reflected solar radiation in the visible and infrared using seven spectral channels. ERS-2 is in a near-polar, sun-synchronous orbit with an equator overpass time of 10:30 in the descending node. ATSR-2 has a 512 km swath width in the nadir, achieving global coverage every three days.

[6] Aerosol and cloud properties are derived using the Oxford/RAL Aerosol and Cloud (ORAC) optimal estimation retrieval scheme that was developed for clouds [*Watts et al.*, 1998] and extended to aerosols [*Marsh et al.*, 2004]. The retrieval scheme averages a block of 12 ATSR-2 pixels to achieve an effective resolution of 2.6 km across-track and 3.5 km along-track. The scheme uses the Discrete Ordinates Radiative Transfer model [*Stammes et al.*, 1988] to calculate the top of atmosphere radiance as a function of the properties of a plane parallel cloud layer or aerosol with an assumed height distribution. ORAC fits the radiance in all channels by varying all retrieved parameters simultaneously, while accounting for a priori information. The scheme also provides error estimates on all retrieved quantities.

[1]School of Geosciences, University of Edinburgh, Edinburgh, UK.
[2]Atmospheric, Oceanic and Planetary Physics, University of Oxford, Oxford, UK.
[3]Rutherford Appleton Laboratory, Didcot, UK.

0094-8276/08/2007GL031394$05.00

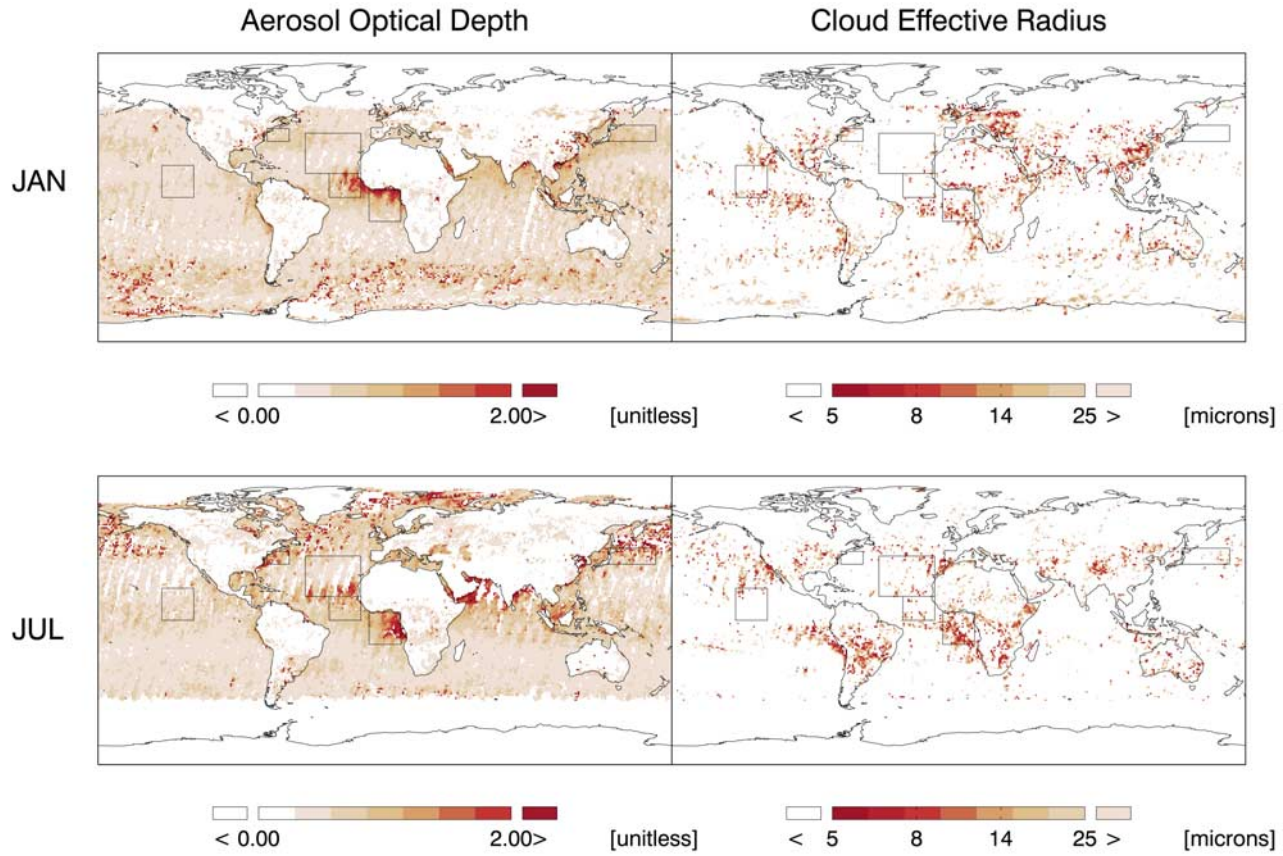

Figure 1. Monthly mean τ_a (unitless) at 0.55 μm and r_e (μm) observed by ATSR-2 onboard ERS-2 during January and July 1997. Data are averaged on a regular $1^\circ \times 1^\circ$ grid with cloud data filtered for cloud top heights <3 km, with an error associated with this measure <200 m, and for 2 μm < r_e < 25 μm. Aerosol data are filtered according to τ_a error <0.25. The striped structure in the plots is an artefact of ATSR-2 sampling. The boxes indicate the regions defined in Table 1.

[7] Cloud flagging is performed prior to retrieval. Over the ocean the difference between the observed thermal radiance and a clear sky value predicted by radiative transfer calculations is used. We also employ an additional test to detect low, warm clouds over the ocean and clouds over land based on surface reflectance at 0.67 and 0.87 μm [*Birks*, 2007]. Cloud properties are retrieved using the 0.67, 0.87, 1.6, 11 and 12 μm channels and the derived products are optical depth at 0.55 μm, effective radius, liquid water path (LWP), cloud top height, pressure and temperature and cloud fraction. Aerosol optical depth at 0.55 μm and aerosol effective radius are retrieved using the 0.67, 0.87 and 1.6 μm channels. The Optical Properties of Aerosol and Clouds (OPAC) inventory provides the a priori information on aerosol optical properties [*Hess et al.*, 1998], with the aerosol type used in each pixel being assigned from aerosol climatology.

[8] Validation of both cloud and aerosol properties derived using the GRAPE algorithm is ongoing [*Poulsen and Watts*, 2002; *Kokhanovsky et al.*, 2007; *Thomas et al.*, 2007a]. We use only retrieved aerosol and cloud data where the retrieval algorithm converged within 10 iterations. For cloud data we use retrievals that have cloud top heights below 3 km (with an error of <200 m), ensuring that we use only low-level clouds that are most likely to be influenced by boundary layer outflow [*Keil and Haywood*, 2003]. Measurements of r_e below 2 μm are removed to prevent contamination of cloud retrievals with erroneously flagged aerosol; r_e values above 25 μm, representing <10% of data, are unrealistic for low-level cloud and have also been filtered from the data. We only consider aerosol retrievals that have τ_a errors <0.25.

3. Results

[9] Figure 1 shows monthly mean values of τ_a and r_e in January and July 1997 averaged on a regular $1^\circ \times 1^\circ$ grid. Observed τ_a values are typically 0–0.8 with the highest values reaching 2 over the eastern Atlantic downwind of Africa. During January there are elevated values of τ_a over the western Pacific, the Arabian Sea, the Bay of Bengal, the South China Sea, the eastern tropical Atlantic, and the Southern Ocean. There are similar distributions of elevated τ_a during July but with smaller values over the western Pacific and higher values over the midlatitude western Atlantic downwind of North America. Values of r_e range from 5 to 25 μm with the smallest values observed over the oceans in regions of continental outflow.

[10] We quantify the Twomey IE over four regions of continental outflow, ensuring a fresh supply of aerosols for cloud droplet formation: eastern equatorial Atlantic (North Africa), eastern South Atlantic (southern Africa), western

Table 1. Seasonal Mean Twomey IE ($-\partial \ln r_e/\partial \ln \tau_a$) and Associated Correlations Between r_e and τ_a During 1997

	Globe[a]		Eastern S. Atlantic[b] (Africa)		Western N. Pacific[c] (Asia)		Western N. Atlantic[d] (North America)		Eastern equation Atlantic[e] (Sahara)		S. Pacific[f]	
Month	IE[g]	r	IE	r	IE	r	IE	r	IE	r	IE	r
DJF	0.13 ± 0.01[h]	−0.75	0.20 ± 0.13[h,k,l]	−0.36	0.12 ± 0.05[h]	−0.68	-0.56 ± 0.13	0.92	0.10 ± 0.02[h]	−0.88	-0.37 ± 0.08	0.65
MAM	0.13 ± 0.01[h]	−0.87	-0.48 ± 0.03	0.38	-0.14 ± 0.01	0.56	0.11 ± 0.11[j]	−0.44	-0.06 ± 0.03	0.74	0.001 ± 0.09[j]	−0.54
JJA	0.16 ± 0.01[h]	−0.99	0.51 ± 0.16[i,k]	−0.85	-0.04 ± 0.05[j]	−0.13	0.16 ± 0.08[h]	−0.78	0.16 ± 0.04[h]	−0.48	-0.16 ± 0.09	−0.50
SON	0.10 ± 0.01[h]	−0.98	$0.27 \pm 0 .05$[h]	−0.85	0.23 ± 0.06[h]	−0.94	-0.16 ± 0.19[j]	0.70	-0.03 ± 0.03[j]	0.64	-0.37 ± 0.07	0.85

[a]Region defined: 180W–180E, 45S–60N; τ_a: r_e correlation = 0.38; AI: r_e correlation = 0.68.
[b]Region defined: 10W–10E, 15S–5N; τ_a: r_e correlation = −0.39; AI: r_e correlation = −0.64.
[c]Region defined: 140E–170E, 35N–45N; τ_a: r_e correlation = −0.47; AI: r_e correlation = −0.36.
[d]Region defined: 60W–74W, 35N–43N; τ_a: r_e correlation = 0.23 AI: r_e correlation = 0.37.
[e]Region defined: 15W–50W, 15N–40N; τ_a: r_e correlation = −0.33; AI: r_e correlation = 0.13.
[f]Region defined: 120W–140W, 0N–20N; τ_a: r_e correlation = −0.17; AI: r_e correlation = 0.16.
[g]To obtain the gradient, r_e was averaged over τ_a size bins of 0.03, between 0.13 and 0.4 in the given region over the period of each season.
[h]An IE consistent with theory assuming $\alpha < 1$.
[i]Regions where $N_d \approx (N_a)^{\alpha}$ cannot be assumed.
[j]Regions where the retrieved IE value is not significant.
[k]The gradient IE was calculated for τ_a values of 0.35–1.5.
[l]Region defined: 15W–35W, 0N–15N.

mid-latitude North Atlantic (North America), and western North Pacific (eastern Asia). We also consider data over the remote Pacific (used as a control), and over the globe. Table 1 defines the geographical regions shown in Figure 1. We find the largest τ_a values over the eastern South Atlantic, downwind of Africa (Figure 1). The southward migration of elevated τ_a over that region during 1997 (not shown) reflects the burning season in Africa, and is consistent with the spatial distribution of ATSR-2 firecounts. In DJF analysis for the eastern South Atlantic is in a box just below the Saharan region (Figure 1) in order to capture this seasonal variation in biomass burning.

[11] Previous studies have argued that aerosol index (AI), a measure of the wavelength dependence of aerosol extinction, is a better quantity to test the Twomey hypothesis because it is sensitive to the fine fraction of aerosol that is more likely to serve as CCN [*Breon et al.*, 2002; *Quaas et al.*, 2004]. AI is not directly retrieved in the GRAPE algorithm but can be approximated by the product of τ_a and the Angström exponent (A). The Angström exponent varies inversely with particle size, the difference between extinction coefficients being greater with smaller particles as determined by Mie scattering. We approximate A using $A \approx \log(b_{ext1}/b_{ext2})/\log(\lambda_1/\lambda_2)$, where λ represents wavelength and b_{ext} represents an extinction coefficient related to a particular aerosol class and effective radius [*Seinfeld and Pandis*, 1998]. Here, we evaluate A at 0.55 and 0.67 μm, where b_{ext} is defined as a function of aerosol effective radius. OPAC classifications give values of b_{ext} according to wavelength, dependent on the mixing ratio of each aerosol component in the aerosol class [*Hess et al.*, 1998]. This mixing ratio is then varied in order to calculate b_{ext} as a function of aerosol effective radius [*Thomas et al.*, 2007b].

[12] A major criticism of using satellite data to test relationships between aerosol and cloud properties has been that these properties are not measured coincidentally [*Avey et al.*, 2007]. Previous studies have used back-trajectories to link cloud and aerosol properties [e.g., *Breon et al.*, 2002], or colocated cloud retrievals and trace gas measurements using a tracer transport model [*Avey et al.*, 2007]. *Breon et al.* [2002] used back-trajectories to couple aerosol and cloud retrievals and found that the distance between measurements is typically less than 100 km. We argue here that analysis of aerosol and cloud properties derived from multi-day and seasonal means averaged at $1 \times 1^{\circ}$ resolution (approximately 100×100 km^2 at low and mid-latitudes) negates the need to couple individual measurements.

[13] Figure 2 shows a time series of τ_a, AI and r_e from 1st December 1996 to 31st January 1998, averaged individually across the six regions defined in Table 1. Standard deviations for daily mean τ_a (AI) range from 0.04 to 0.06 (0.01–0.05), but can reach up to 0.2 for τ_a and AI in strong continental outflow. Standard deviations for r_e typically range from 4 to 6 μm. The 28-day rolling mean reduces the random noise on the daily means. All regions that include continental outflow show coherent variations in aerosol and cloud properties. The timing of the maximum values of τ_a and AI are consistent with prior knowledge of outflow patterns, e.g. outflow over the western Atlantic is at a maximum between June and August [*Quinn and Bates*, 2003]. There is little variation in τ_a or AI over the remote Pacific, with values much less than those observed in continental outflow, as expected.

[14] The differences between τ_a and AI provide an indication of whether aerosols are present mainly in the coarse (>1 μm) or fine (<1 μm) mode, as explained above. Figure 2 shows that τ_a is elevated above AI over the western Pacific in late spring when there is strong outflow from the Asian continent that typically includes mineral dust transport events [*Kim et al.*, 2006; NOAA National Centers for Environmental Prediction, NCEP reanalysis electronic atlas, 2007, available at http://www.cdc.noaa.gov/ncep_reanalysis/]. A similar discrepancy between τ_a and AI occurs over the equatorial Atlantic downwind of the Sahara throughout the year but is most pronounced between February and April, consistent with AI retrievals from the Total Ozone Mapping Spectrometer. In contrast, North American outflow over the Atlantic shows similar values for τ_a and AI, suggesting that fine aerosols dominate that outflow. Variation of r_e depends on region. The smallest values occur over the eastern Atlantic where we see large increases in τ_a. In general, regions that include continental outflow show a negative relationship between τ_a or AI and r_e, consistent with the Twomey IE. The region downwind of southern Africa shows the strongest anti-correlation between

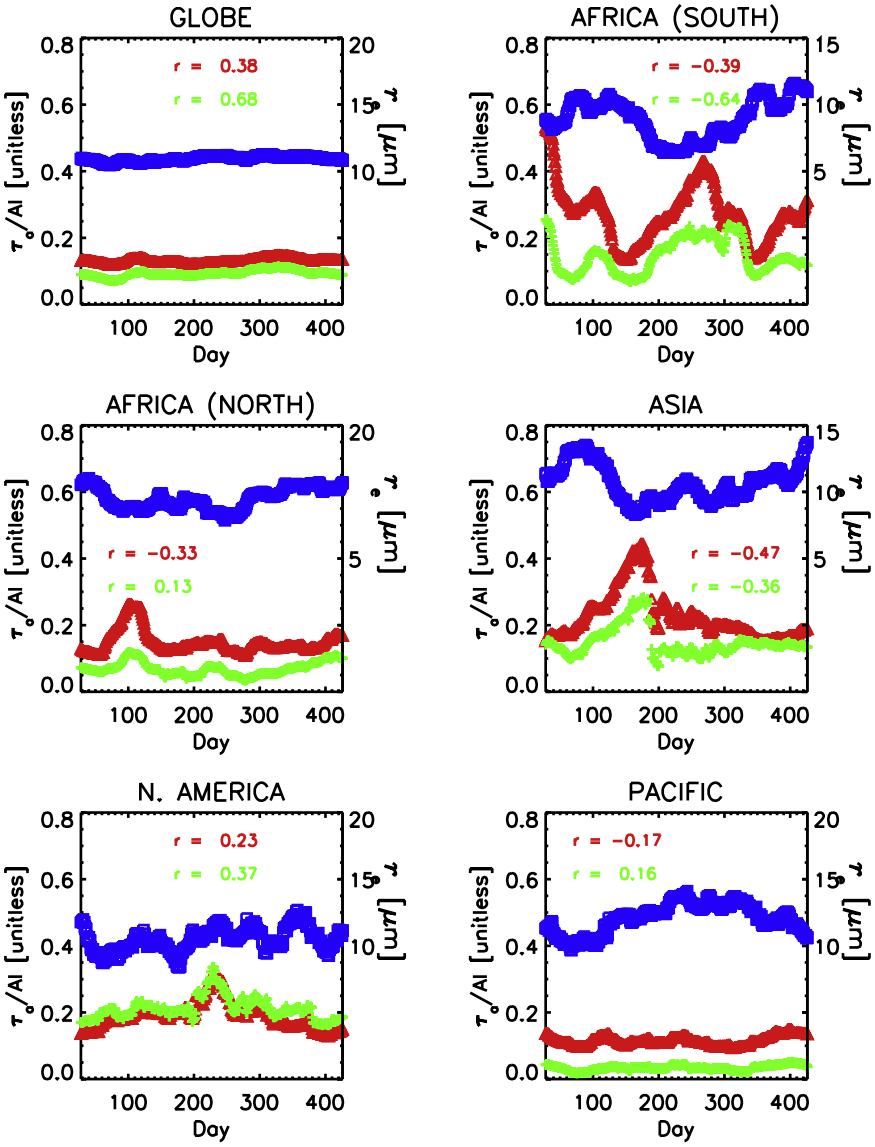

Figure 2. 28-day rolling mean of τ_a at 0.55 μm (red) and r_e (μm, blue) observed by ATSR-2 between 1st December 1996 and 31st January 1998 over the globe, eastern South Atlantic, eastern equatorial Atlantic, western North Pacific, western North Atlantic, and the South Pacific. AI (green) is calculated using offline extinction coefficients at 0.55μm and 0.67 μm. Standard errors (standard deviation $/\sqrt{(n-2)}$) are superimposed on the time series but are close to zero. Correlation coefficients between τ_a/AI (red/green) and r_e are given in each panel.

AI and r_e (r = −0.64). For other regions the correlation between τ_a or AI and r_e over 1997 is much weaker (Table 1), partly due to the seasonal nature of continental outflow from many regions.

[15] Similar anti-correlations could be generated from systematic sampling errors. Erroneous cloud flagging, identifying high aerosol loading as cloudy pixels, would result in very low values of r_e with elevated τ_a. It is likely that such a situation would be identified by a bi-modal distribution in r_e measurements, which is not observed in the GRAPE data. Aerosol and cloud layers may be decoupled across a frontal system or if the atmosphere is vertically stable [*Sinha et al.*, 2003] and in such situations anti-correlations between τ_a and r_e do not signal a causal relationship. However, coastal regions, typified by low-level cloud, experience cycling between stratiform and cumuliform cloud layers [*Paluch and Lenschow*, 1991] so we expect aerosol and cloud properties to be related over the spatial scales studied.

[16] The Twomey IE can be described as the relative change in r_e associated with a relative change in τ_a [*Feingold et al.*, 2001]: $-\partial \ln r_e/\partial \ln \tau_a$. Assuming a homogeneous cloud with a constant LWP, the relationship between cloud droplet number (N_d) and the aerosol number concentration (N_a) is nonlinear: $N_d \propto N_a^{\alpha}$, where α is a unitless parameter that provides an indication of particle hygroscopicity, with low values corresponding to low hygroscopicity. A characteristic α value adopted by several previous studies is 0.7 [*Breon et al.*, 2002; *Feingold et al.*, 2003]; below, we look at the sensitivity of α to the interpretation of our results. As previously discussed, AI may provide a better proxy for N_a [*Breon et al.*, 2002; *Quaas et al.*, 2004], but our analysis

concentrates on τ_a because AI is not a GRAPE retrieval product. It can be shown that $r_e \propto \tau_a^{-\alpha/3}$ [*Feingold et al.*, 2003] so using $\alpha = 0.7$ gives IE = $\alpha/3 \approx 0.23$.

[17] Table 1 shows the monthly mean values of IE and the associated correlation (r) between τ_a and r_e for the defined regions. The gradients are calculated for τ_a between 0.13 and 0.4 with r_e averaged over τ_a increments of 0.03, accounting for the standard error of the measurements in each size bin. Values of $\tau_a > 0.4$ are noisy, due to few observations above this threshold, with the exception of southern Africa where aerosol loading during the burning season is much greater than in other regions; consequently we calculate IE for between 0.35 and 1.5 for DJF and JJA.

[18] A physical condition of the assumed relationship between N_d and N_a is $\alpha \leq 1$ so that $0 \leq IE \leq 0.33$. On a global scale, GRAPE data yields seasonal mean IE values between 0.10 and 0.16 corresponding to values of α ranging from 0.30 to 0.48. The theoretical value of IE = 0.23 (assuming $\alpha = 0.7$) is based only on the physical relationship between aerosol number and cloud droplet number, disregarding other important physical processes including aerosol size distribution and updraft velocity [*Feingold et al.*, 2001]. Previous studies have shown a similar range of IE values when using this assumption [e.g., *Feingold et al.*, 2003].

[19] Over the western North Atlantic, IE is strongest in JJA when continental outflow is greatest. Over the western North Pacific the strongest IE is not observed during the period of maximum outflow (MAM) when mineral dust is prevalent [*Kim et al.*, 2006] but during DJF/SON when dust does not dominate the outflow. Over the eastern South Atlantic we find significant IE values for DJF, JJA, and SON; there is only a small amount of active burning during MAM (ATSR World Fire Atlas, http://dup.esrin.esa.it/ionia/wfa/index.asp, 2007). During JJA, we find the IE is 0.51, implying an unphysical value of $\alpha > 1$. The high correlation coefficient (-0.85) associated with this season suggests that the observed relationship is not due to noisy data. In regions of high aerosol loading using the assumption $N_d \approx N_a^{\alpha}$ may be an oversimplification. Feedback mechanisms associated with drizzle suppression at the base of the cloud result in increased air entrainment from above the cloud. Aerosol entrainment and activation may be enhanced depending on the humidity of air above the cloud and the consequent effect on the LWP [*Ackerman et al.*, 2004]. During DJF we use the equatorial region to study African burning outflow as noted above. Significant IE is found both here and in the adjacent outflow region downwind of the Sahara desert, and we conclude that is difficult to separate dust and burning outflow in this region although burning is more likely responsible for the IE in this season. A weak IE is seen in the adjacent Saharan region during JJA.

[20] There are of course limitations to the theory outlined by *Twomey* [1974] and the analysis approach we adopt in this paper, which we outline below. Recent work has highlighted that the Twomey theory describes only the physical relationship between aerosol number and cloud microphysics [*Feingold et al.*, 2001, 2003]. Other physical effects are not taken into account, most notably aerosol size distribution, which is estimated to describe ~80% of the variability in aerosol activation [*Duesk et al.*, 2006]. Although thought to take a secondary role, aerosol chemical composition is also important in determining α and hence IE [*Duesk et al.*, 2006]. Aerosols must be hygroscopic in order to act as CCN; hydrophobic aerosol types such as desert dust need to obtain a hydrophilic coating (e.g. sulphur or organics). Smaller aerosols from industrial sources and biomass burning that contain organic species tend to be hygroscopic and more immediately effective as CCN [*Seinfeld and Pandis*, 1998].

[21] The Twomey hypothesis is based on the assumption that the cloud layer has a homogenous LWC. Over the spatial scales measured by the satellite these assumptions are unlikely to be valid: cycling between stratus layers and cumuli clouds will lead to inhomogeneity [*Paluch and Lenschow*, 1991]. Air circulation within the cloud, possibly modified by aerosol feedback mechanisms, will also result in changing LWC [*Ackerman et al.*, 2004]. The uncertainties in the derived IE values in Table 1 are likely be underestimated because we do not account for variations in LWC over the spatial scales studied. Despite the many assumptions we have made our results are quantitatively consistent with theory at a global scale, and regionally consistent during periods of high continental outflow.

[22] **Acknowledgments.** CEB is supported by NERC DARC studentship NER/S/D/2006/14345, and via additional support from the Rutherford Appleton Laboratory. The Oxford authors wish to acknowledge NERC funding NER/T/S/2001/00205 and NE/B503933/1.

References

Ackerman, A. S., et al. (2004), The impact of humidity above stratiform clouds on indirect aerosol climate forcing, *Nature*, *432*, 1014–1017.

Albrecht, B. A. (1989), Aerosols, cloud microphysics, and fractional cloudiness, *Science*, *245*(4923), 1227–1230.

Avey, L., T. J. Garrett, and A. Stohl (2007), Evaluation of the aerosol indirect effect using satellite, tracer transport model, and aircraft data from the International Consortium for Atmospheric Research on Transport and Transformation, *J. Geophys. Res.*, *112*, D10S33, doi:10.1029/2006JD007581.

Birks, A. (2007), Improvements to the AATSR IPF relating to land surface temperature retrieval and cloud clearing over land, technical note, ESA, Paris.

Breon, F. M., et al. (2002), Aerosol effect on cloud droplet size monitored from satellite, *Science*, *295*, 834–838.

Duesk, U., et al. (2006), Size matters more than chemistry for cloud-nucleating ability of aerosol particles, *Science*, *312*, 1375–1378.

Feingold, G., L. A. Remer, J. Ramaprasad, and Y. J. Kaufman (2001), Analysis of smoke impact on clouds in Brazilian biomass burning regions: An extension of Twomey's approach, *J. Geophys. Res.*, *106*(D19), 22,907–22,922.

Feingold, G., W. L. Eberhard, D. E. Veron, and M. Previdi (2003), First measurements of the Twomey indirect effect using ground-based remote sensors, *Geophys. Res. Lett.*, *30*(6), 1287, doi:10.1029/2002GL016633.

Hess, M., et al. (1998), Optical properties of aerosols and clouds: The software package OPAC, *Bull. Am. Meteorol. Soc.*, *79*(5), 831–844.

Intergovernmental Panel on Climate Change (IPCC) (2007), *Climate Change 2007: The Physical Basis of Climate Change. Contribution of Working Group 1 to the Fourth Assessment Report of the Intergovernmental Panel on Climate Change*, edited by S. Solomon et al., Cambridge Univ. Press, New York.

Keil, A., and J. M. Haywood (2003), Solar radiative forcing by biomass burning aerosol particles during SAFARI 2000: A case study based on measured aerosol and cloud properties, *J. Geophys. Res.*, *108*(D13), 8467, doi:10.1029/2002JD002315.

Kim, S.-W., S.-C. Yoon, J. Kim, and S.-Y. Kim (2006), Seasonal and monthly variations of columnar aerosol optical properties over east Asia determined from multi-year MODIS, LIDAR, and AERONET Sun/Sky radiometer measurements, *Atmos. Environ.*, *4*, 1634–1651.

Kokhanovsky, A. A., et al. (2007), Aerosol remote sensing over land: A comparison of satellite retrievals using different algorithms and instruments, *Atmos. Res.*, *85*(3–4), 372–394.

Marsh, S. H., et al. (2004), An optimal estimation aerosol retrieval scheme for ATSR-2, memorandum, Atmos. Oceanic and Planet. Phys., Dep. of Phys., Univ. of Oxford, Oxford, U. K.

Paluch, I. R., and D. H. Lenschow (1991), Stratiform cloud formation in the marine boundary layer, *J. Atmos. Sci.*, *48*(19), 2141–2158.

Poulsen, C., and P. Watts (2002), Retrieval and validation of cloud properties using ATSR-2 data, paper presented at Meteorological Satellite Conference, EUMETSAT, Dublin, 2–6 Sep.

Quaas, J., O. Boucher, and F.-M. Bréon (2004), Aerosol indirect effects in POLDER satellite data and the Laboratoire de Météorologie Dynamique–Zoom (LMDZ) general circulation model, *J. Geophys. Res.*, *109*, D08205, doi:10.1029/2003JD004317.

Quinn, P. K., and T. S. Bates (2003), North American, Asian, and Indian haze: Similar regional impacts on climate?, *Geophys. Res. Lett.*, *30*(11), 1555, doi:10.1029/2003GL016934.

Seinfeld, J. H., and S. N. Pandis (1998), *Atmospheric Chemistry and Physics: From Air Pollution to Climate Change*, John Wiley, Hoboken, N. J.

Sinha, P., P. V. Hobbs, R. J. Yokelson, D. R. Blake, S. Gao, and T. W. Kirchstetter (2003), Distributions of trace gases and aerosols during the dry biomass burning season in southern Africa, *J. Geophys. Res.*, *108*(D17), 4536, doi:10.1029/2003JD003691.

Stammes, K., et al. (1988), A numerically stable algorithm for discrete-ordinate-method radiative transfer in multiple scattering and emitting layered media, *Appl. Opt.*, *27*, 2502–2509.

Thomas, G. E., et al. (2007a), Comparison of AATSR and SEVIRI aerosol retrievals over the northern Adriatic, *Q. J. R. Meteorol. Soc.*, *133*(S1), 85–95.

Thomas, G. E., et al. (2007b), An optimal estimation aerosol retrieval scheme for (A)ATSR, memorandum, Atmos. Oceanic and Planet. Phys., Dep. of Phys., Univ. of Oxford, Oxford, U. K.

Twomey, S. (1974), Pollution and the planetary albedo, *Atmos. Environ.*, *8*, 1251–1256.

Watts, P. D., et al. (1998), Study on cloud properties derived from Meteosat second generation observations, *Rep. 97/181*, EUMETSAT, Darmstadt, Germany.

Watts, P. D., et al. (2000), Aerosol properties derived from Meteosat second generation, *Rep. EUM.004*, EUMETSAT, Darmstadt, Germany.

C. P. G. Arnold, E. Campmany, E. Carboni, R. G. Grainger, and G. E. Thomas, Atmospheric, Oceanic and Planetary Physics, University of Oxford, Clarendon Laboratory, Parks Road, Oxford OX1 3PU, UK.

C. E. Bulgin and P. I. Palmer, School of Geosciences, University of Edinburgh, King's Buildings, West Mains Road, Edinburgh EH9 3JW, UK. (paul.palmer@ed.ac.uk)

B. N. Lawrence, C. Poulsen, and R. Siddans, Rutherford Appleton Laboratory, Didcot OX11 0QX, UK.